

## **Analysis, Design and Implementation of a Quasi-Proportional-Resonant Controller for a Multifunctional Capacitive-Coupling Grid-Connected Inverter**

Ye, Tao; Dai, Ning-Yi; Lam, Chi-Seng; Wong, Man-Chung; Guerrero, Josep M.

*Published in:*  
I E E Transactions on Industry Applications

*DOI (link to publication from Publisher):*  
[10.1109/TIA.2016.2581152](https://doi.org/10.1109/TIA.2016.2581152)

*Publication date:*  
2016

*Document Version*  
Early version, also known as pre-print

[Link to publication from Aalborg University](#)

*Citation for published version (APA):*  
Ye, T., Dai, N.-Y., Lam, C.-S., Wong, M.-C., & Guerrero, J. M. (2016). Analysis, Design and Implementation of a Quasi-Proportional-Resonant Controller for a Multifunctional Capacitive-Coupling Grid-Connected Inverter. *I E E Transactions on Industry Applications*, 52(5), 4269 - 4280. <https://doi.org/10.1109/TIA.2016.2581152>

### **General rights**

Copyright and moral rights for the publications made accessible in the public portal are retained by the authors and/or other copyright owners and it is a condition of accessing publications that users recognise and abide by the legal requirements associated with these rights.

- Users may download and print one copy of any publication from the public portal for the purpose of private study or research.
- You may not further distribute the material or use it for any profit-making activity or commercial gain
- You may freely distribute the URL identifying the publication in the public portal -

### **Take down policy**

If you believe that this document breaches copyright please contact us at [vbn@aub.aau.dk](mailto:vbn@aub.aau.dk) providing details, and we will remove access to the work immediately and investigate your claim.



# Analysis, Design and Implementation of a Quasi-Proportional-Resonant Controller for a Multi-Functional Capacitive-Coupling Grid-Connected Inverter

Tao Ye<sup>1</sup>, NingYi Dai<sup>1</sup>, Chi-Seng Lam<sup>2</sup>, Man-Chung Wong<sup>1,2</sup>, Josep M. Guerrero<sup>3</sup>

1. Electrical and Computer Engineering Department, University of Macau, Macau, P.R. China

2. State Key Laboratory of Analog and Mixed-Signal VLSI, University of Macau, Macau, P.R. China

3. Department of Energy Technology, Aalborg University, Denmark

**Abstract**—The capacitive-coupling grid-connected inverter (CGCI) is coupled to the point of common coupling via a second-order LC branch. Its operational voltage is much lower than that of a conventional inductive-coupling grid-connected inverter (IGCI) when it serves as a multifunctional inverter to compensate reactive power and transfer active power simultaneously. It is a promising solution for micro-grid and building-integrated distributed generator systems. A quasi-proportional-resonant (quasi-PR) controller is applied to reduce steady-state current tracking errors of the CGCI in this paper. The quasi-PR controller generates the voltage reference for use of carrier-based pulse width modulation, which can effectively reduce output current ripples. The second-order coupling impedance of the CGCI causes its modeling and controller design to differ from that of the conventional IGCI. A comprehensive design method for the quasi-PR controller in a CGCI is developed. The quasi-PR controller is also compared with a proportional-integration current controller. Simulation results are provided to verify the effectiveness of the quasi-PR controller and its design method in a CGCI. The current tracking errors are greatly reduced when the quasi-PR controller rather than the proportional-integration controller is applied. Experimental results are also provided to validate the CGCI as a multifunctional grid-connected inverter.

**Keywords**—Active power; Capacitive-coupling grid-connected inverter; Proportional-integration controller; Quasi-PR controller; reactive power

## I. INTRODUCTION

The increasing need for more effective and environmentally friendly electrical power systems plays an important role in the development of a smart grid [1]-[4]. The grid-connected inverter is the key element for efficient use of distributed energy resources. Recently, increasing attention has been paid to multifunctional grid-connected inverters, which can provide auxiliary services to enhance power quality [5], [6] in addition to providing active power transfer. Previous research on grid-connected inverters has mainly used an LC-type or LCL-type filter to reduce output current distortion [7], [8]. This type of grid-connected inverter is called an inductive-coupling grid-connected inverter (IGCI) in this paper because the fundamental

frequency coupling impedance is inductive [9]-[11]. The IGCI usually requires a high DC-link voltage because its operational voltage should be higher than the grid voltage to transfer active power and perform power quality conditioning.

A capacitive-coupling grid-connected inverter (CGCI) was also proposed [12], [13]. The CGCI is coupled to the grid via an inductor in series with a capacitor. The fundamental frequency impedance of its coupling branch is capacitive. This topology was first proposed under the name of hybrid filter [14]-[17], and it has shown its advantage in reducing operational voltage under certain circumstances. The CGCI can transfer active power and inject leading reactive power into a grid with an operational voltage lower than the grid voltage [17]-[21]. The required DC-link voltage is much lower than that of the IGCI. As a result, the CGCI appears to be a promising solution for building-integrated photovoltaic generation systems or small-scale micro-grids. It can be coupled to a low-voltage DC bus to provide reactive power and inject active power into an AC grid.

As aforementioned, the capacitive-coupling inverter was first named as hybrid active filter (HAPF) and was used to damp harmonic resonance in industrial power system [14]-[17]. The inverter output voltage reference is obtained by amplifying harmonic current by a gain  $K$ . Then carrier-based pulse width modulation (PWM) or space vector modulation is used. The following study was concerned with the fundamental frequency reactive power control capability of the HAPF. Since the previous voltage reference is not applicable, current tracking directly with hysteresis PWM was adopted to control the LC-HAPF [18]-[21]. This method is simple and easy to implement. However, the sampling rate for the current must be high enough to track the reference current accurately. At the same time, the hysteresis PWM method has the drawbacks of widely varying switching frequency and large current ripples. The carrier-based PWM can fix the variability of switching frequency and reduce output current distortion. However, a voltage reference needs

to be generated for controlling the CGCI, so it can use carrier-based PWM [6], [7], [10], [11], [22]-[24].

A current controller could convert current reference to voltage reference. The proportional ( $P$ ) current controller was used to derive the voltage reference in CGCI [12]. A  $P$ -unit current controller was proposed for the CGCI [13], which is equivalent to a proportional ( $P$ ) controller in the  $s$ -domain and is equivalent to a proportional-integral ( $PI$ ) controller in the  $z$ -domain. A high gain must be used to guarantee the performance of the current controller, which does not meet stability margin requirements. In addition, the parameters are selected by trying and testing. Hence, a current controller with better performance should be applied.

PI and proportional-resonant (PR) controllers are the two most widely used current controllers for IGCI [6]-[11], [24]-[28]. The conventional PI controller is not capable of eliminating steady-state errors in current tracking [9], [22], [24], [29], especially when an LC or LCL filter is coupled to the inverter. A synchronous PI controller was proposed to achieve theoretical zero steady-state errors for a three-phase inverter, in which stationary-frame AC quantities are transformed to DC quantities [22], [30]. However, additional computations are required to coordinate the transformation when this method is applied to the single-phase IGCI. A stationary-frame PR controller has the same operational principle as a synchronous-frame PI controller when it is applied to the conventional single-phase IGCI [22], [31], [32]. Compared to the stationary-frame PR controller, a quasi-PR controller can avoid the stability problems associated with an infinite gain and reduce the sensitivity toward slight frequency variation [31], [33].

Sliding mode control (SMC) can provide attractive features such as fast transient response and applicable to multivariable systems. But its chattering problems may lead to low steady state accuracy, especially when switching frequency is not high enough [34]-[37]. Repetitive control (RC) can be employed to improve tracking accuracy by placing an internal model into the loop. The dynamic response of RC is much slower than that of a feedback controller such as PI or PR controller [38]-[39]. Many other advanced controllers have been proposed, such as adaptive sliding mode control, improved repetitive control, model predictive control, fuzzy logic control (FLC) and artificial neural network control (ANNC) [40]-[44]. These control methods could be more robust under system parameter variations and could achieve fast transient response. However, more efforts are required to implement these controllers. It is a time-consuming task to realize them on a digital controller using C/C++ language. What's more, the performance of adaptive based control, FLC and ANNC are also related to the available training data.

As the first step to improve the current controller of the CGCI, a quasi-PR current controller is applied to control the CGCI for the first time, which can achieve zero steady-state error at the selected oscillation frequency with relatively

small gain. The second-order coupling impedance of the CGCI causes its control model to differ from that of the conventional IGCI. The system response after applying the quasi-PR controller to the CGCI will be studied for parameter selection, which has not been done before. A comprehensive design method for the quasi-PR controller will also be developed.

The operational principle of the CGCI is briefly introduced in Section II, followed by the mathematical model of its current control loop. The design of the quasi-PR controller for a CGCI is presented in Section III, in which a comparison with the PI current controller is also given. Simulation results for a CGCI with the quasi-PR controller are given for comparison with those with the PI controller in Section IV. The experimental results are provided in Section V. Finally, conclusions are drawn in Section VI.

## II. MODELING OF THE CGCI

### A. Operational principle of the CGCI

The circuit configuration of a single-phase CGCI is shown in Fig. 1, where  $v_s$  and  $V_{inv}$  denote grid voltage and inverter output voltage, and  $i_s$ ,  $i_L$  and  $i_c$  are source, load and compensating currents, respectively.  $L_c$  and  $C_c$  are the coupling inductor and capacitor, respectively, and  $C_{dc}$  is the DC-link capacitor.

The power flow ( $P_{inj}$  and  $Q_{inj}$ ) between the voltage source inverter and the grid can be calculated as follows [45]:

$$P_{inj} = \left( \frac{V_s V_{inv}}{Z} \cos \delta - \frac{V_s^2}{Z} \right) \cos \theta + \frac{V_s V_{inv}}{Z} \sin \delta \sin \theta \quad (1)$$

$$Q_{inj} = \left( \frac{V_s V_{inv}}{Z} \cos \delta - \frac{V_s^2}{Z} \right) \sin \theta - \frac{V_s V_{inv}}{Z} \sin \delta \cos \theta \quad (2)$$

In (1) and (2),  $\delta$  represents the phase angle between  $V_s$  and  $V_{inv}$ . The values of  $Z$  and  $\theta$  are determined by the coupling impedance of the grid-connected inverter, which can be expressed as:

$$X_c = Z \angle \theta = -j \frac{1}{\omega C_c} + j \omega L_c = -j \frac{1}{\omega C} = \frac{1}{\omega C} \angle -90^\circ \quad (3)$$

The power base is introduced as follows:

$$S_{base} = V_s^2 \cdot \omega C \quad (4)$$

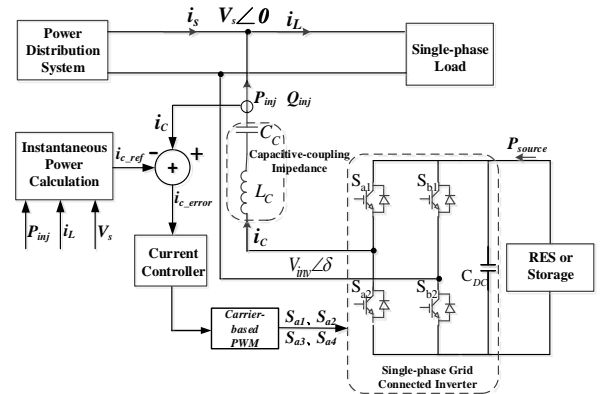


Fig. 1. Circuit configuration of a single-phase CGCI

By combining (1) to (4), the normalized output voltage of the CGCI is calculated as in (5), and its variation in normalized power flow can be plotted in three dimensions as shown in Fig. 2.

$$\frac{V_{inv}}{V_s} = \sqrt{\left(\frac{P_{inj}}{S_{base}}\right)^2 + \left(\frac{Q_{inj}}{S_{base}} - 1\right)^2} \quad (5)$$

According to analyses in previous works [12], [13], the inverter operational voltage is lower when its output reactive power varies in the vicinity of  $S_{base}$ . Thus, it is better to connect the CGCI to the point of common coupling (PCC), at which continuous reactive power compensation is required for inductive loadings such as in water pumps and centralized air-conditioning systems, etc. Under this situation, the CGCI can simultaneously inject active power from a distributed source to the grid while keeping its operational voltage low.

When the CGCI is used to transfer active power from the renewable energy sources and compensate reactive power at the PCC simultaneously, the output current reference is calculated as follows:

$$i_{c\_ref} = \frac{1}{v_m} \begin{bmatrix} \sin \theta & \cos \theta \end{bmatrix} \begin{bmatrix} P_{source} \\ q_L \end{bmatrix} \quad (6)$$

where  $P_{source}$  represents the active power from distributed generators.  $q_L$  is the load reactive power extracted by using the instantaneous reactive power theory [12], [13].

#### B. Modeling the current control loop of the CGCI

A current control loop is adopted to control the output current of the CGCI to track the current reference, as illustrated in Fig. 3. The carrier-based PWM method is used. Its corresponding mathematical model is deduced as given in Fig. 4.

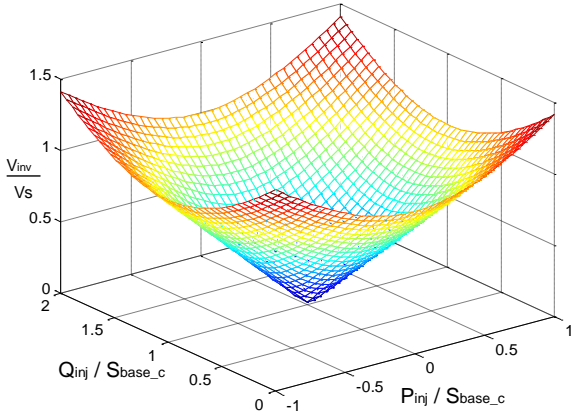


Fig. 2. Inverter output voltage versus active and reactive power flow

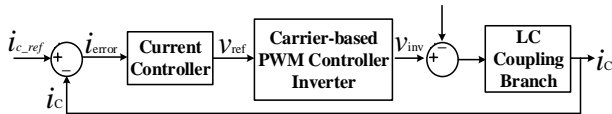


Fig. 3. Current control loop block diagram of the CGCI

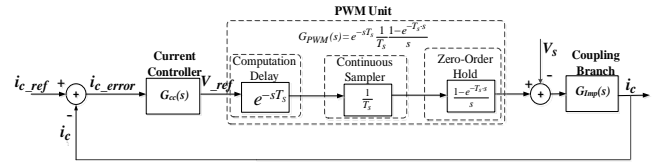


Fig. 4. S-domain model of the current control loop of the CGCI

The mathematical model of each block in Fig. 4 is as follows.

#### ■ Current Controller: $G_{cc}(s)$

As mentioned in the previous section, current controllers with different characteristics have been developed for conventional grid-connected inverters, which are coupled to the grid via inductive impedance. A current control is designed for controlling the CGCI, which is analyzed in detail in the next section.

#### ■ PWM Unit: $G_{PWM}(s)$

In an average  $s$ -domain model, the PWM converter can be simplified to a unity gain. However, the computation time of the digital controller cannot be negligible [9], [46]-[48]. To accurately describe the effects of time delay on the CGCI controller, the computation delay, sampler and zero-order hold as an  $s$ -domain PWM unit model are used as shown in Fig. 4. The  $s$ -domain transfer function of the PWM unit can be expressed as

$$G_{PWM}(s) = \frac{e^{-T_s \cdot s} (1 - e^{-T_s \cdot s})}{T_s \cdot s} \quad (7)$$

where  $T_s$  is the sampling period. To accurately reveal digital implementation effects and obtain a rational transfer function, delays are usually approximated by poles and zeros [49]-[52]. A proper way to accomplish this is to use the *Pade'* approximation. The first-order *Pade'* approximation shown in (8) can maintain the  $s$ -domain analysis with fair agreement between simplicity and accuracy.

$$e^{-T_s \cdot s} \approx \frac{1 - 0.5 \cdot T_s \cdot s}{1 + 0.5 \cdot T_s \cdot s} = \text{Pade}' \quad (8)$$

Substituting (8) into (7) yields:

$$G_{PWM}(s) = \frac{e^{-T_s \cdot s} (1 - e^{-T_s \cdot s})}{T_s \cdot s} \approx \frac{1 - 0.5 \cdot T_s \cdot s}{(1 + 0.5 \cdot T_s \cdot s)^2} \quad (9)$$

#### ■ Coupling Impedance: $G_{Imp}(s)$

The LC coupling branch of the CGCI can be expressed as:

$$G_{Imp}(s) = \frac{C_c s}{L_c C_c s^2 + 1} \quad (10)$$

According to Fig. 4, the overall transfer function of the CGCI controller is obtained as:

$$I_c(s) = G_{cc}(s) G_{PWM}(s) G_{Imp}(s) I_{c\_ref}(s) - G_{vs\_c} V_s(s) \quad (11)$$

$$= \frac{G_{cc}(s) G_{PWM}(s) G_{Imp}(s)}{1 + G_{cc}(s) G_{PWM}(s) G_{Imp}(s)} I_{c\_ref}(s) - \frac{G_{Imp}(s)}{1 + G_{cc}(s) G_{PWM}(s) G_{Imp}(s)} V_s(s)$$

where  $G_{cref\_c}(s)$  is the system closed-loop transfer function between  $i_c$  and  $i_{c\_ref}$ , and  $G_{vs\_ic}(s)$  is the closed-loop system transfer function between  $i_c$  and  $V_s$ .  $G_{Quasi-PR}(s)G_{PWM}(s)G_{Imp}(s)$  is the open-loop transfer function.

### III. DESIGN OF A QUASI-PR CONTROLLER FOR THE CGCI

#### A. Quasi-PR Controller for the CGCI

A quasi-PR controller is used as the current controller in Fig. 4. Its transfer function is expressed as:

$$G_{cc}(s) = G_{Quasi-PR}(s) = K_p + \frac{2K_r\omega_c s}{s^2 + 2\omega_c s + \omega_0^2} \quad (12)$$

Three parameters need to be selected for a quasi-PR current controller to simplify the parameters tuning procedure. The typical design scenario can be summarized as follows.

- An appropriate  $\omega_c$  should be chosen to give a satisfactory bandwidth around the resonant frequency.
- $K_p$  should be chosen such that good transient response and stability are guaranteed.
- $K_r$  is chosen so that phase and magnitude steady-state errors are eliminated.

On the basis of the power quality standards of Macau and Hong Kong (CEM supply rules, HKE and CLP supply rules of Hong Kong), the standard limit of frequency variation is  $\pm 2\%$  [57], [58]. Assuming that the frequency variation margin is  $\pm 2\%$ , then  $\omega_c$  can be designed as  $\omega_c = 2\pi \cdot 50 \cdot 2\% = 6.28$ .

$K_p$  should be high enough to obtain high gain at the fundamental frequency and the low-order harmonic frequency. However, the stability margin may be sacrificed when the  $K_p$  value is increased. The boundary of the  $K_p$  value is determined by using Routh's stability criterion. The open-loop transfer function of the related closed-loop transfer function  $G_{cref\_c}(s)$  is  $G_{Quasi-PR}(s)G_{PWM}(s)G_{Imp}(s)$  and assume that  $G_{cref\_c}(s) = N(s)/D(s)$ . Then, the characteristic equation can be obtained:

$$D(s) + KN(s) = 0 \quad (13)$$

where  $K$  indicates the upper boundary of the proportional gain under different  $K_p$  values. It is assumed that the delay time of the PWM unit is just half of the sampling period ( $0.5T_s$ ); then, the corresponding boundary of  $K_p$  can be deduced as follows:

$$K_p \leq \frac{8 \cdot L_c}{3 \cdot T_s} \quad (14)$$

The value of  $K_r$  is adjusted to limit the steady-state error. For example, the magnitude of  $G_{Quasi-PR}(s)G_{PWM}(s)G_{Imp}(s)$  needs to be higher than 100 to decrease the current tracking error to less than 1% according to (11) and without considering the effect of grid-side voltage  $V_s$ . Both  $K_r$  and  $K_p$  are adjusted to satisfy this requirement and simultaneously guarantee enough stability margin.

In summary, the design procedures of the quasi-PR controller for a CGCI are as follows.

1) According to the power quality standard, select the value of  $\omega_c$ .

$$\omega_c = 2 \cdot \pi \cdot f_0 \cdot \Delta f \quad (15)$$

where  $f_0$  is the fundamental frequency, and  $\Delta f$  is the standard limit of the frequency variation.

2) Calculate the upper boundary of the controller's proportional gain  $K_p$  according to (14). Select a value of  $K_p$  within this boundary.

3) Set a small value for  $K_r$ , which can guarantee that the magnitude response of the open-loop transfer function at the designed resonant frequency (50 Hz) is above 40 dB.

4) Adjust the  $K_p$  value within its boundary so that the magnitude response of closed-loop transfer function  $G_{cref\_c}(s)$  approaches 0 dB and its phase response approaches 0 degrees at the fundamental frequency. Meanwhile, the frequency response of  $G_{cref\_c}(s)$  should provide adequate attenuation of any high-frequency interference signal.

5) The value of  $K_r$  is adjusted to ensure that the magnitude response of  $G_{cref\_c}(s)$  at high frequencies, especially around 10 KHz, is well suppressed.

6) The magnitude response of closed-loop transfer function  $G_{vs\_c}(s)$  is evaluated to guarantee enough attenuation to the grid-side voltage disturbances.

#### B. Design Verification of the Parameters

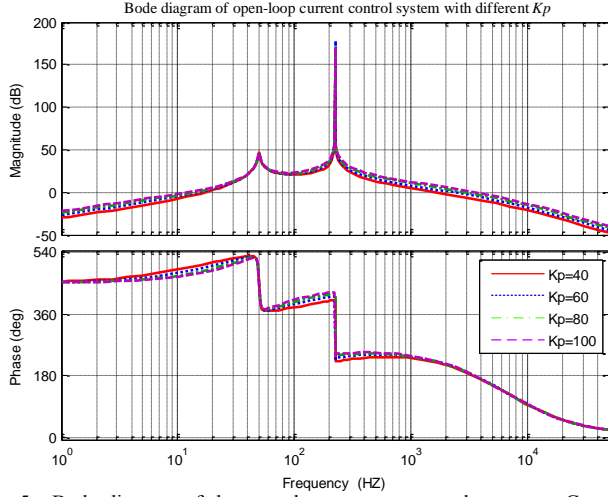
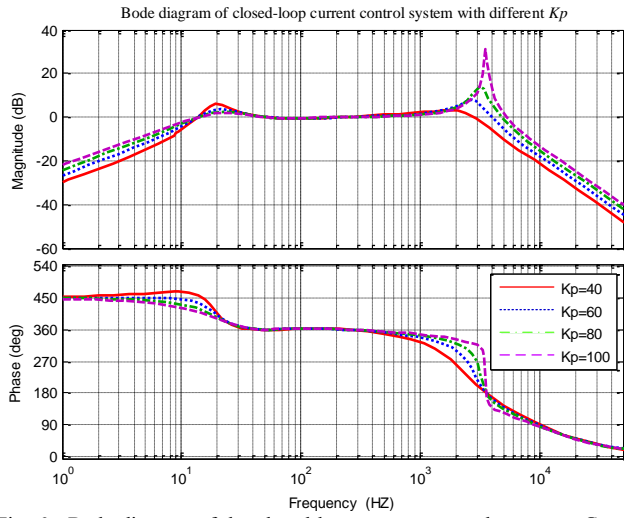
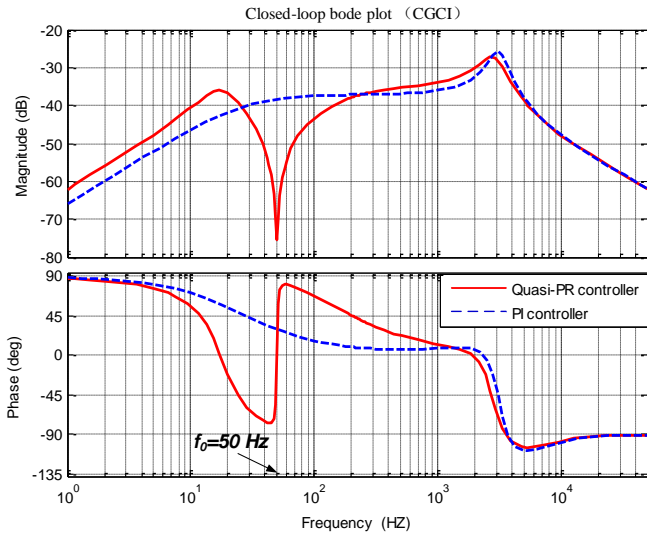
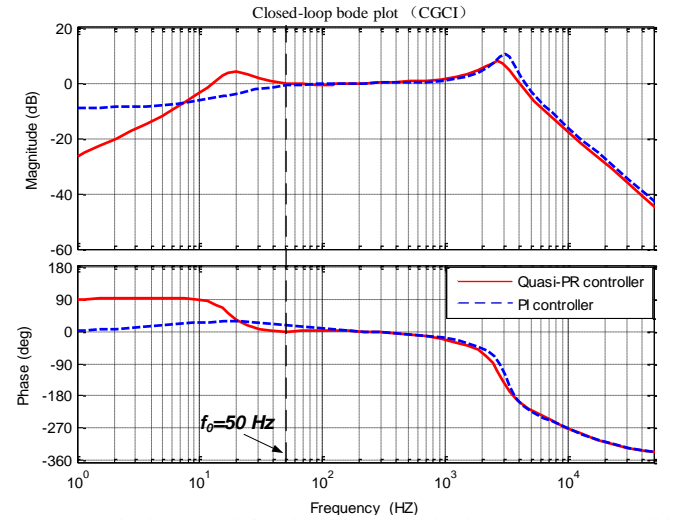
The model of the current control loop is analyzed by using MATLAB. The system parameter settings of the CGCI are given in TABLE I. According to (14), the  $K_p$  value should be smaller than 106. The selected parameters for the quasi-PR controller and the PI controller are also listed in TABLE I. Bode diagrams of the open-loop and closed-loop current control systems are shown in Fig. 5 and Fig. 6, respectively.

It can be concluded from Fig. 5 that the open-loop gain at the designed resonant frequency (50 Hz) is above 40 dB. Hence, the closed-loop response of  $G_{cref\_c}(s)$  achieves unity gain with zero phase shifting at the designed resonant frequency. To illustrate the effect of  $K_p$  on the frequency response, curves obtained by using four different  $K_p$  values are shown in Fig. 5 and Fig. 6. In case the stability margin can be satisfied, a higher  $K_p$  results in good current tracking performance at the fundamental frequency response. However, to attenuate the high-frequency interference signal simultaneously, a  $K_p$  value of around 60 is a better choice according to Fig. 6.

The Bode diagram of closed-loop transfer function  $G_{vs\_c}(s)$  is shown in Fig. 7. The results indicate that the designed current control loop with the quasi-PR controller provides enough attenuation to the disturbance from the grid-side voltage. That is, the distortion component in the grid-side voltage will not be amplified by the CGCI, even though its coupling circuit is a second-order LC branch.

TABLE I. SELECTED PARAMETERS FOR MATLAB SIMULATION

	Parameters	Value
System settings	Switching frequency $f_s$	10 kHz
	Fundamental frequency	50 Hz
	Filter inductor $L_C$	4 mH
	Filter capacitor $C_C$	125 $\mu$ F
Quasi-PR controller	$K_r=5800$ ; $K_p=50$ ; $\omega_c=6.28$ ;	
PI controller	$K_p=72$ ; $K_i=4200$	
PR controller	$K_r=5800$ ; $K_p=50$ ;	

Fig. 5. Bode diagram of the open-loop current control system –  $G_{\text{Quasi-PR}}(s)G_{\text{PWM}}(s)G_{\text{Imp}}(s)$  with  $\omega_c=5$ ,  $K_r=5000$  and different  $K_p$ Fig. 6. Bode diagram of the closed-loop current control system –  $G_{\text{ref}_c}(s)$  with  $\omega_c=5$ ,  $K_r=5000$  and different  $K_p$ Fig. 7. Bode diagram of the closed-loop transfer functions  $G_{v_{s,c}}(s)$  (solid line: PI controller; dashed line: Quasi-PR controller)Fig. 8. Bode diagram of the closed-loop transfer function  $G_{\text{ref}_c}(s)$  (solid line: PI controller; dashed line: quasi-PR controller)

### C. Comparison Between the PI Controller and Quasi-PR Controller

In this section, a comparison between application of the PI controller and the quasi-PR controller to CGCI is performed. The PI controller is expressed as follows:

$$G_{CC}(s) = G_{PI}(s) = K_p + \frac{K_i}{s} \quad (16)$$

By substituting (16) as the current controller into (11), the  $s$ -domain closed-loop transfer function with the PI controller is obtained. The system parameters of this controller are listed in TABLE I. The Bode diagram of  $G_{v_{s,c}}(s)$  is also shown in Fig. 7 when PI controller is adopted. This controller also provides good attenuation of the grid voltage disturbances.

The Bode diagram of  $G_{\text{ref}_c}(s)$  by using the PI controller and quasi-PR controller is shown in Fig. 8. A zoomed view of this figure in the vicinity of the fundamental frequency is shown in Fig. 9. The current tracking error is clearly reduced when the quasi-PR controller is used, especially at the fundamental frequency. Increasing the  $K_p$  of the PI controller may force the magnitude response to approach zero. However, a large gain could cause the control system to become unstable and weaken its capability to attenuate high-frequency interference signals. The quasi-PR control uses a lower  $K_p$  value, which meets the aforementioned stability margin requirement and design criterion.



## IV. SIMULATION RESULTS

### A. Simulation Setting

To verify the effectiveness of the quasi-PR controller for the CGCI, a set of simulation tests are carried out by using PSCAD/EMTDC. The control block diagram is shown in Fig. 11. Table II lists the simulated system parameters, in which the DC-link voltage of the inverter is supplied by an ideal DC voltage source. The CGCI simultaneously injects active power from the external sources into the grid and compensates reactive power of the loads. The DC-link voltage is lower than the grid voltage when the CGCI is used.

The comparison mainly focuses on the steady-state performance. Thus, the performances are conducted with respect to the following parameters:

- Source current total harmonic distortion ( $THD_{is}$ ) at the steady-state situation.
- Active power error

$$P_{error} = |P_{source} - P_{inj}| / P_{source} \quad (18)$$

where  $P_{inj}$  is the output active power of the CGCI, and  $P_{source}$  is the active power reference, which is set in the simulation to model the output of the external sources.

- Reactive power error

$$Q_{error} = |Q_{Load} - Q_{inj}| / Q_{Load} \quad (19)$$

where  $Q_{inj}$  is the output reactive power of the CGCI and  $Q_{load}$  is the reactive power of loads connected to the PCC.

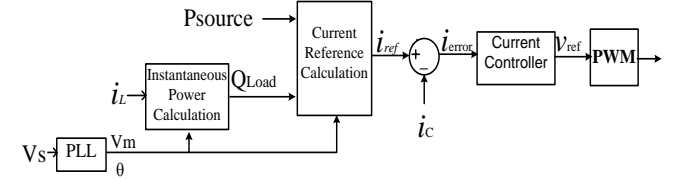


Fig. 11. Control block diagram of the CGCI

TABLE II. SYSTEM PARAMETER SETTINGS IN THE SIMULATION

System parameters	
Grid parameters	Value
Grid voltage $V_s$	220 V
Fundamental frequency $f_0$	50 Hz
Sampling frequency	20 KHz
Source inductor $L_s$	0.001 mH
Inverter parameters	Value
DC link capacitor $C_{dc}$	1 mF
Filter inductor $L_c$	4 mH
Filter capacitor $C_c$	125 $\mu$ F
Linear load ('//': parallel structure; '+': cascaded structure)	
DC link voltage $V_{dc}$	170 V
Linear load 1 (0.5 s-0.7 s)	15 $\Omega$ // (120 mH + 8 $\Omega$ )
Linear load 2 (0.1 s-0.3 s)	20 $\Omega$ // (6 mH + 10 $\Omega$ )
Linear load 3 (0.3 s-0.5 s)	28 $\Omega$ // (4 mH + 8 $\Omega$ )

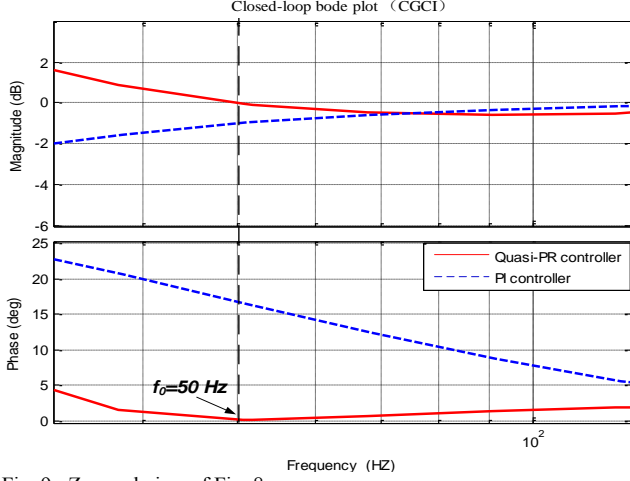


Fig. 9. Zoomed view of Fig. 8.

### D. Comparison Between the PR Controller and the Quasi-PR Controller

In this section, a study is carried out to compare the PR controller and the quasi-PR controller. Both of these two controllers have not been applied to CGCI in early work. A PR controller is expressed as follows:

$$G_{cc}(s) = G_{PR}(s) = K_p + \frac{2K_r s}{s^2 + \omega_0^2} \quad (17)$$

The system parameters of the PR controller are listed in TABLE I. The coefficient  $K_p$  and  $K_r$  are set to the same value as that of the quasi-PR controller. The Bode diagram of the open-loop current control system with the PR controller and the quasi-PR controller is shown in Fig.10. It can be concluded that a PR controller introduces an infinite gain at the system frequency (50Hz). The gain of the quasi-PR controller is finite, but still relatively high for reducing steady-state error. In addition, the bandwidth of the quasi-PR controller can be widened by adjusting the parameter  $\omega_c$ , so that the sensitivity towards slight frequency variation in a utility grid is reduced [53]-[56].

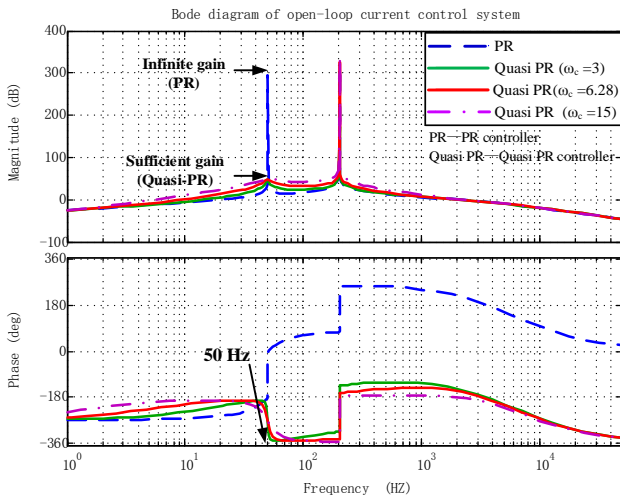


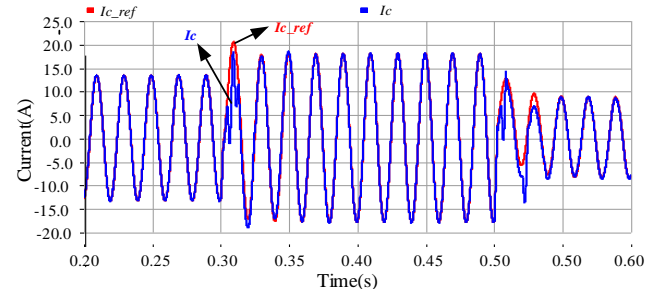
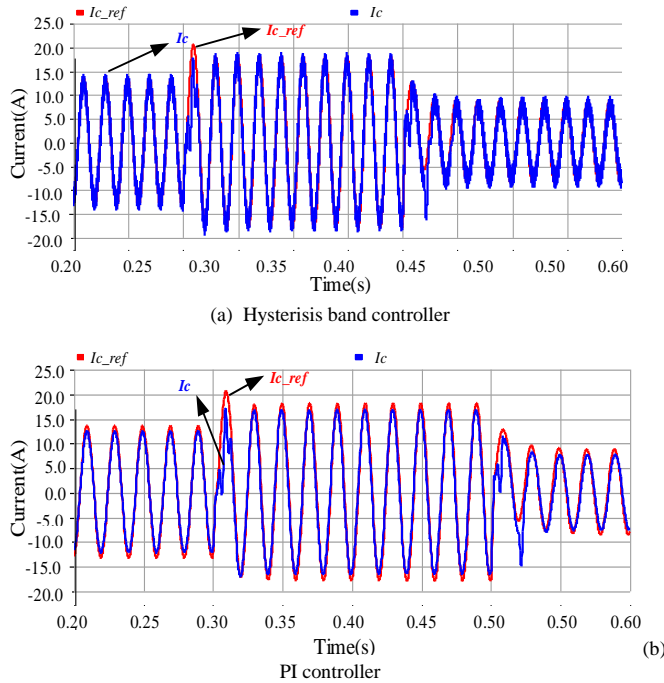
Fig. 10. Bode diagram of the open-loop current control system



### B. Comparisons of steady state performance

The quasi-PR controller is used as the current controller to generate a reference voltage for the carrier-based PWM. In order to illustrate the effectiveness of the quasi-PR controller in reducing steady-state current tracking error, the hysteresis band controller [18], [19] and PI controller are also used in the simulation. The hysteresis band controller could directly control the output current of the inverter to tracking its reference. Simulation results are shown in Fig. 12 to Fig. 14, respectively. The current reference and output current of the CGCI are shown in Fig. 12. Voltage and current waveforms and  $THD_{is}$  variations are shown in Fig. 13. The active power and reactive power variations are provided in Fig. 14.

The system performance indexes at the steady state are summarized in Tables III, IV and V. It can be concluded that the current tracking error is reduced by using the quasi-PR controller. The hysteresis band controller and the PI controller cannot eliminate the steady-state current tracking errors. A similar case also occurs when the PI controller is applied to control an IGCI [6], [9], [11], [22], [25]-[27], [31]. As a result, both the active and reactive power outputs of the CGCI cannot track the reference with high accuracy. When the quasi-PR controller is used, however, both the active and reactive power tracking errors are lower. Moreover, the source current distortion is also lower. It can be concluded that the quasi-PR controller with carrier-based PWM is the better choice for use with the CGCI to achieve nearly zero steady-state current tracking errors.



(c) Quasi-PR controller  
Fig. 12 Current tracking waveforms

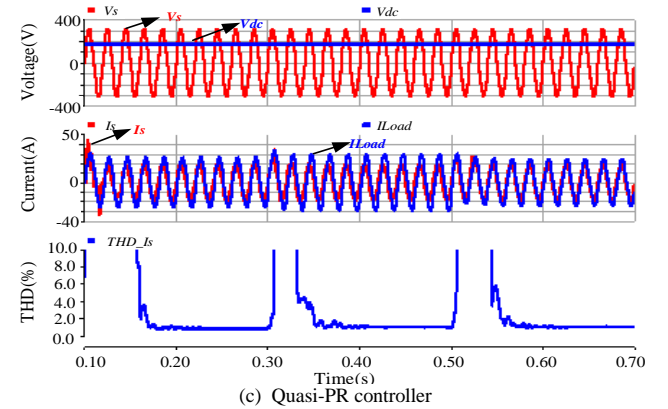
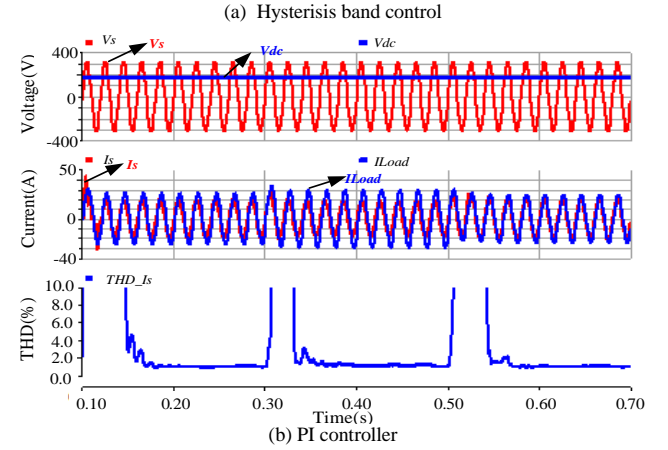
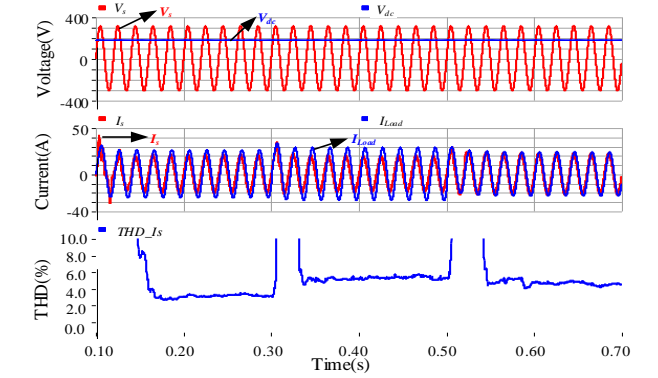


Fig. 13 Voltage and current waveforms and source current THD

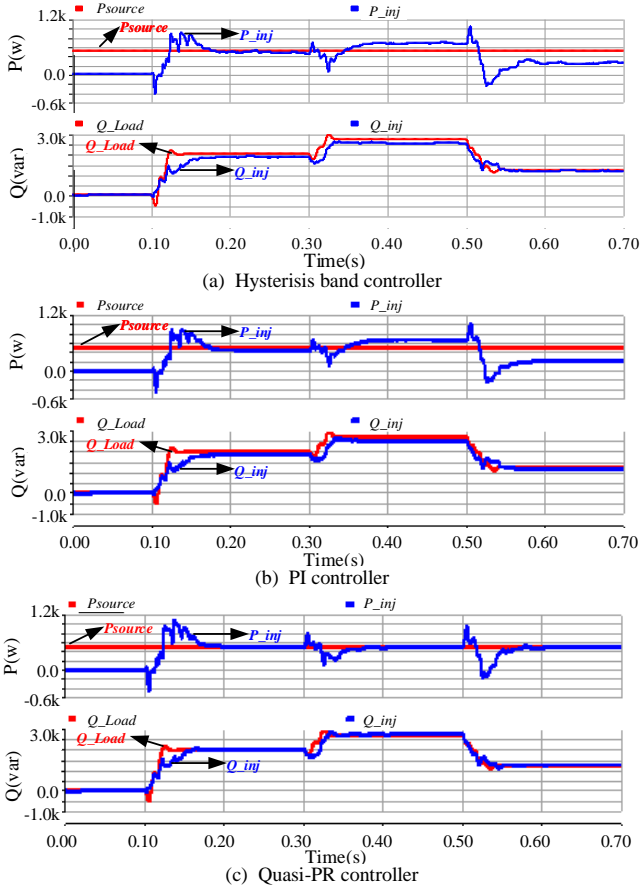


Fig. 14 Active power and reactive power

TABLE III. STEADY-STATE PERFORMANCE USING HYSTERESIS BAND CONTROLLER

Hysteresis band control							
Time	THD <sub>is</sub> (%)	P <sub>inj</sub> (W)	P <sub>source</sub> (W)	Q <sub>inj</sub> (var)	Q <sub>load</sub> (var)	P <sub>error</sub> (%)	Q <sub>error</sub> (%)
0.29s	3.02	447.50	500	1879.24	2002.3	10.5	6.15
0.49s	4.99	646.91	500	2548.65	2738.78	29.38	6.94
0.69s	4.53	260.08	500	1157.7	1227.64	47.98	5.70

TABLE IV. STEADY-STATE PERFORMANCE USING THE PI CONTROLLER

PI controller (K <sub>p</sub> =72, K <sub>i</sub> =4500)							
Time	THD <sub>is</sub> (%)	P <sub>inj</sub> (W)	P <sub>source</sub> (W)	Q <sub>inj</sub> (var)	Q <sub>load</sub> (var)	P <sub>error</sub> (%)	Q <sub>error</sub> (%)
0.29s	0.95	439.39	500	1855.86	2002.29	12.12	7.31
0.49s	1.09	659.07	500	2510.47	2738.77	31.81	8.34
0.69s	1.10	214.17	500	1178.07	1227.64	57.17	4.04

TABLE V. STEADY-STATE PERFORMANCE USING THE QUASI-PR CONTROLLER

Quasi-PR controller (K <sub>p</sub> =50, ω <sub>c</sub> =6.28, K <sub>r</sub> =5800)							
Time	THD <sub>is</sub> (%)	P <sub>inj</sub> (W)	P <sub>source</sub> (W)	Q <sub>inj</sub> (var)	Q <sub>load</sub> (var)	P <sub>error</sub> (%)	Q <sub>error</sub> (%)
0.29s	0.84	500.12	500	2021.64	2002.3	0.02	0.97
0.49s	0.99	499.94	500	2761.53	2738.78	0.01	0.83
0.69s	1.02	482.22	500	1257.3	1227.64	3.56	2.42

### C. Comparisons between the PR controller and the Quasi-PR controller under system frequency variations

A comparison between the PR controller and the quasi-PR controller are conducted. Both of these two controllers could reduce the steady-state current tracking error at fundamental frequency. The quasi-PR controller widens the band-width at the resonant frequency, as illustrated in Fig. 10. Therefore, their performance is compared under system frequency variations. The simulation results are listed in Table VIII and Table IX when the system frequency is set to 49.1 Hz. Result indicates that the performance of the quasi-PR controller is slightly better under system frequency variation. Since the quasi-PR controller can provide sufficient gain in a wider band near the designed resonant frequency (50Hz), it is selected to control the CGCI in this paper.

TABLE VI. STEADY-STATE PERFORMANCE USING THE PR CONTROLLER WHEN SYSTEM FREQUENCY IS 49.1 HZ

Time	THD <sub>is</sub> (%)	P <sub>inj</sub> (W)	P <sub>source</sub> (W)	Q <sub>inj</sub> (var)	Q <sub>load</sub> (var)	P <sub>error</sub> (%)	Q <sub>error</sub> (%)
0.29s	2.43	495.28	500	2086.63	2020.23	0.94	3.29
0.49s	4.52	539.52	500	2834.38	2756.35	7.90	2.83
0.69s	2.84	474.84	500	1309.52	1246.72	5.03	5.04

TABLE VII. STEADY-STATE PERFORMANCE USING THE QUASI-PR CONTROLLER WHEN SYSTEM FREQUENCY IS 49.1 HZ

Time	THD <sub>is</sub> (%)	P <sub>inj</sub> (W)	P <sub>source</sub> (W)	Q <sub>inj</sub> (var)	Q <sub>load</sub> (var)	P <sub>error</sub> (%)	Q <sub>error</sub> (%)
0.29s	2.44	496.05	500	2084.51	2020.23	0.79	3.18
0.49s	4.49	535.84	500	2831.69	2756.35	7.17	2.73
0.69s	2.82	478.05	500	1307.92	1246.72	4.39	4.91

## V. EXPERIMENTAL RESULTS

A single-phase CGCI experimental prototype was designed and constructed in the laboratory, and its system parameters are listed in Table VIII. The control algorithm is implemented in a DSP-TMS320F28335. A photo of the experimental prototype is shown in Fig. 15. The grid-side voltage is scaled down to 110 V due to limitations of the laboratory facilities.

The parameters of the quasi-PR controller ( $K_p=50$ ,  $\omega_c=5$ ,  $K_r=5800$ ) are designed according to the proposed parameter design procedures described in Section III. The experimental results of the CGCI are evaluated with the same performance parameters as used in the previous simulation case. The DC voltage is set to 85 V, which is lower than the grid-side voltage of 110 V. The active power reference is set at 90 W, and a linear inductive load is used.

TABLE VIII. EXPERIMENTAL SYSTEM SETTINGS

Item	Value
Capacitor C <sub>c</sub>	120.95 μF
Inductor L <sub>c</sub>	3.791 μH
Grid voltage V <sub>s</sub>	110 Vrms, 50 Hz
DC-link voltage	85 V
Active power transfer	90 W
Linear load	14 Ω, 25.27 mH

Fig. 16 shows the experimental results (load-side, CGCI-side and source-side results) when the PI controller with carrier-based PWM is used, and Fig. 17 shows the experimental results when the quasi-PR controller is applied in CGCI. The experimental results are summarized in Table IX. It can be concluded that the power tracking errors are greatly reduced when the quasi-PR controller is used instead of the PI controller in CGCI. The source current distortion is also lower. The validity and effectiveness of the application the quasi-PR controller to be CGCI and its design method are thus proved.

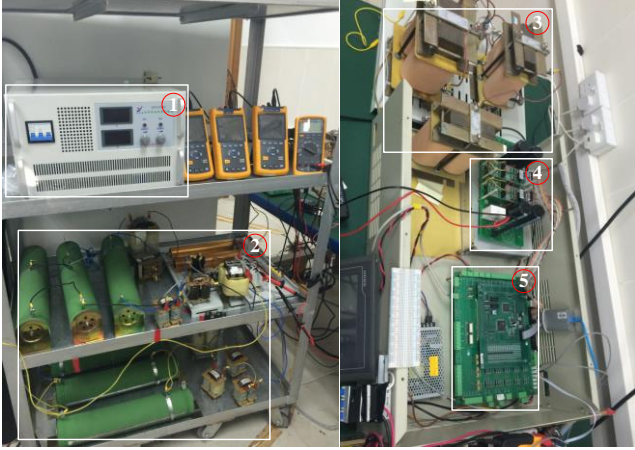


Fig. 15. Experimental prototype of a single-phase CGCI. ① DC power supply, ② Loads, ③ Coupling impedance, ④ IGBT and drivers, ⑤ Control board and signal conditioning circuit.

TABLE IX. EXPERIMENTAL RESULTS

	THD <sub>is</sub> (%)	P <sub>inj</sub> (W)	P <sub>source</sub> (W)	Q <sub>inj</sub> (Kvar)	Q <sub>load</sub> (Kvar)	P <sub>error</sub> (%)	Q <sub>error</sub> (%)
PI	3.1	64	90	0.465	0.45	28.89	0.0333
PR	1.9	97	90	0.456	0.47	7.78	0.0298

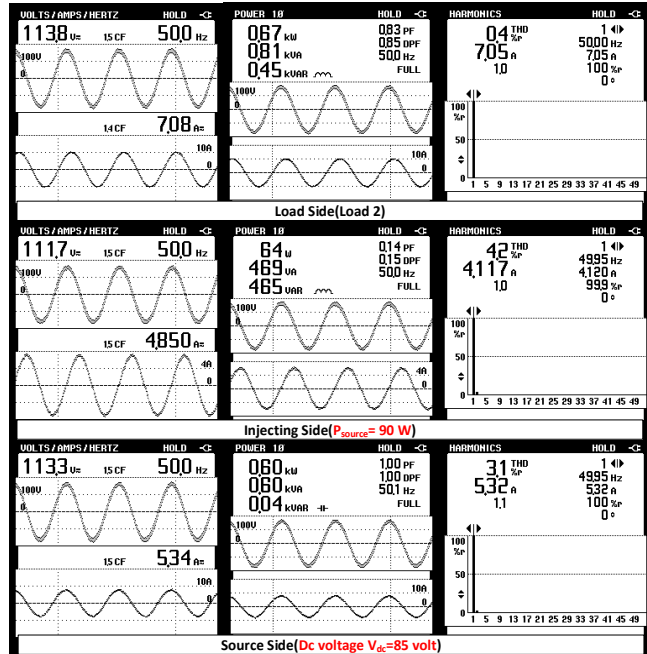


Fig. 16. Experimental results of the PI controller with carrier-based PWM

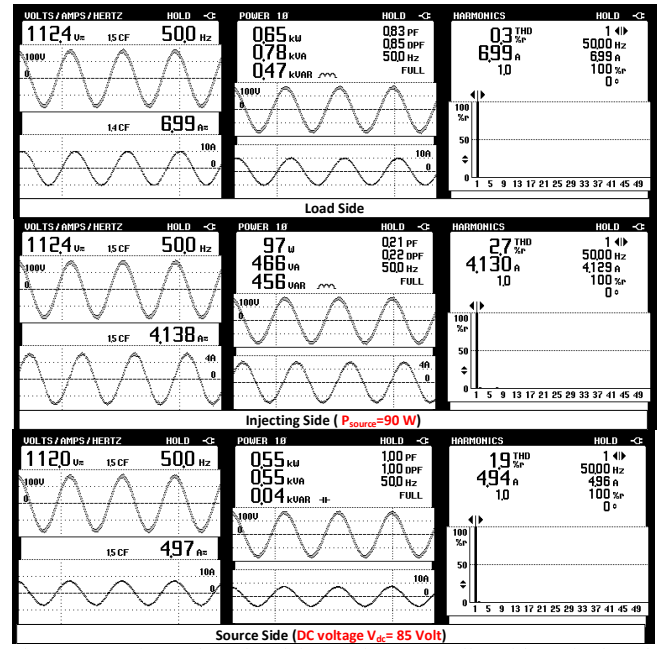


Fig. 17. Experimental results of the quasi-PR controller with carrier-based PWM

## VI. CONCLUSION

The CGCI can inject active power into the grid and compensate reactive power with an operational voltage lower than grid voltage. It is a promising alternative to a grid-connected inverter in a building-integrated distributed generator system or micro-grid. The CGCI is coupled to the grid via a second-order LC branch. Therefore, the mathematical model and current controller for a traditional IGC cannot be directly applied to the CGCI. A quasi-PR controller is applied to the CGCI to reduce the steady-state current tracking error. A corresponding control parameter design method is proposed. Both simulation and experimental results are provided to validate the proposed controller and its design. Comparison with a PI controller is also provided. The results show that the quasi-PR controller is the better choice to fulfill the requirements of active power and reactive power injection with low source current THD.

## ACKNOWLEDGMENT

The authors would like to thank the Science and Technology Development Fund, Macao SAR Government for financial support of project (072/2012/A3) and the University of Macau for financial support of projects (MRG014/DNY/2013/FST) and (MYRG2015-00084-FST).

## REFERENCES

- [1] V. K. N. Lau and D. H. K. Tsang, "Optimal Energy Scheduling for Residential Smart Grid With Centralized Renewable Energy Source," *IEEE Syst. J.*, vol. 8, no. 2, pp. 562–576, Jun. 2014.
- [2] C. K. Lee, B. Chaudhuri, and S. Y. Hui, "Hardware and Control Implementation of Electric Springs for Stabilizing Future Smart Grid With Intermittent Renewable Energy Sources," *IEEE J. Emerg. Sel. Top. Power Electron.*, vol. 1, no. 1, pp. 18–27, Mar. 2013.
- [3] V. Salehi, A. Mohamed, A. Mazloomzadeh, and O. A. Mohammed, "Laboratory-Based Smart Power System, Part I: Design and System

- Development," *IEEE Trans. Smart Grid*, vol. 3, no. 3, pp. 1394–1404, Sep. 2012.
- [4] A. Izadian, N. Girrens, and P. Khayyer, "Renewable Energy Policies: A Brief Review of the Latest U.S. and E.U. Policies," *IEEE Ind. Electron. Mag.*, vol. 7, no. 3, pp. 21–34, Sep. 2013.
  - [5] H. Calleja and H. Jimenez, "Performance of a Grid Connected PV System Used as Active Filter," *Energy Convers. Manag.*, vol. 45, no. 15–16, pp. 2417–2428, Sep. 2004.
  - [6] Z. Zeng, H. Yang, R. Zhao, and C. Cheng, "Topologies and Control Strategies of Multi-Functional Grid-Connected Inverters for Power Quality Enhancement: A Comprehensive Review," *Renew. Sustain. Energy Rev.*, vol. 24, pp. 223–270, Aug. 2013.
  - [7] B. Hoff and W. Sulkowski, "Grid-Connected VSI With LCL Filter—Models and Comparison," *IEEE Trans. Ind. Appl.*, vol. 50, no. 3, pp. 1974–1981, May 2014.
  - [8] A. Reznik, M. G. Simoes, A. Al-Durra, and S. M. Mueyen, "LCL Filter Design and Performance Analysis for Grid-Interconnected Systems," *IEEE Trans. Ind. Appl.*, vol. 50, no. 2, pp. 1225–1232, Mar. 2014.
  - [9] X. Zhang, J. W. Spencer, and J. M. Guerrero, "Small-Signal Modeling of Digitally Controlled Grid-Connected Inverters With LCL Filters," *IEEE Trans. Ind. Electron.*, vol. 60, no. 9, pp. 3752–3765, Sep. 2013.
  - [10] W. Wu, Y. He, and F. Blaabjerg, "An LLCL Power Filter for Single-Phase Grid-Tied Inverter," *IEEE Trans. Power Electron.*, vol. 27, no. 2, pp. 782–789, Feb. 2012.
  - [11] Z. Zou, Z. Wang, and M. Cheng, "Modeling, Analysis, and Design of Multifunction Grid-Interfaced Inverters With Output LCL Filter," *IEEE Trans. Power Electron.*, vol. 29, no. 7, pp. 3830–3839, Jul. 2014.
  - [12] W.-C. Zhang, N.-Y. Dai, and M.-C. Wong, "Capacitive-coupled grid-connected inverter with active power injection ability," in *7th International Power Electronics and Motion Control Conference*, 2012, vol. 3, pp. 1639–1645.
  - [13] N.-Y. Dai, W.-C. Zhang, M.-C. Wong, J. M. Guerrero, and C.-S. Lam, "Analysis, control and experimental verification of a single-phase capacitive-coupling grid-connected inverter," *Power Electronics, IET*, vol. 8, pp. 770–782, 2015.
  - [14] S. Sriathumrong and H. Akagi, "Medium-voltage transformerless ac/dc power conversion system consisting of a diode rectifier and a shunt hybrid filter," *IEEE Trans. Ind. Appl.*, vol. 39, no. 3, pp. 874–882, May 2003.
  - [15] R. Inzunza and H. Akagi, "A 6.6-kV Transformerless Shunt Hybrid Active Filter for Installation on a Power Distribution System," *IEEE Trans. Power Electron.*, vol. 20, no. 4, pp. 893–900, Jul. 2005.
  - [16] H. Akagi, "Active Harmonic Filters," *Proceedings of the IEEE*, vol. 93, no. 12, pp. 2128–2141, Dec. 2005.
  - [17] S. Ostroznik, P. Bajec, and P. Zajec, "A Study of a Hybrid Filter," *IEEE Trans. Ind. Electron.*, vol. 57, no. 3, pp. 935–942, Mar. 2010.
  - [18] C. S. Lam, M. C. Wong, and Y. D. Han, "Hysteresis current control of hybrid active power filters," *Power Electronics, IET*, vol. 5, pp. 1175–1187, 2012.
  - [19] C.-S. Lam, W.-H. Choi, M.-C. Wong, and Y.-D. Han, "Adaptive DC-Link Voltage-Controlled Hybrid Active Power Filters for Reactive Power Compensation," *IEEE Trans. Power Electron.*, vol. 27, no. 4, pp. 1758–1772, Apr. 2012.
  - [20] Chi-Seng Lam and Man-Chung Wong, *Design and control of hybrid active power filter*. Springer Briefs in Electrical and Computer Engineering, Springer, Jan. 2014, pp. 39–60.
  - [21] W. Lei, L. Chi-Seng, and W. Man-Chung, "An adaptive hysteresis band controller for LC-coupling hybrid active power filter with approximate constant switching frequency," in *Power and Energy Engineering Conference (APPEEC), 2014 IEEE PES Asia-Pacific*, 2014, pp. 1–5.
  - [22] Y. Li, D. M. Vilathgamuwa, and P. C. Loh, "Microgrid Power Quality Enhancement Using a Three-Phase Four-Wire Grid-Interfacing Compensator," *IEEE Trans. Ind. Appl.*, vol. 41, no. 6, pp. 1707–1719, Nov. 2005.
  - [23] Y. Yang, H. Wang, and F. Blaabjerg, "Reactive Power Injection Strategies for Single-Phase Photovoltaic Systems Considering Grid Requirements," *IEEE Trans. Ind. Appl.*, vol. 50, no. 6, pp. 4065–4076, Nov. 2014.
  - [24] L. Herman, I. Papic, and B. Blazic, "A Proportional-Resonant Current Controller for Selective Harmonic Compensation in a Hybrid Active Power Filter," *IEEE Trans. Power Deliv.*, vol. 29, no. 5, pp. 2055–2065, Oct. 2014.
  - [25] D. N. Zmood, D. G. Holmes, and G. H. Bode, "Frequency-Domain Analysis of Three-Phase Linear Current Regulators," *IEEE Trans. Ind. Appl.*, vol. 37, no. 2, pp. 601–610, 2001.
  - [26] F. Blaabjerg, R. Teodorescu, M. Liserre, and A. V. Timbus, "Overview of Control and Grid Synchronization for Distributed Power Generation Systems," *IEEE Trans. Ind. Electron.*, vol. 53, no. 5, pp. 1398–1409, Oct. 2006.
  - [27] S. Yang, Q. Lei, F. Z. Peng, and Z. Qian, "A Robust Control Scheme for Grid-Connected Voltage-Source Inverters," *IEEE Trans. Ind. Electron.*, vol. 58, no. 1, pp. 202–212, Jan. 2011.
  - [28] Z. Yao and L. Xiao, "Control of Single-Phase Grid-Connected Inverters With Nonlinear Loads," *IEEE Trans. Ind. Electron.*, vol. 60, no. 4, pp. 1384–1389, Apr. 2013.
  - [29] M. P. Kazmierkowski and L. Malesani, "Current Control Techniques for Three-Phase Voltage-Source PWM Converters: A Survey," *IEEE Trans. Ind. Electron.*, vol. 45, no. 5, pp. 691–703, 1998.
  - [30] F. Briz, M. Degner, and R. Lorenz, "Dynamic Analysis of Current Regulators for AC Motors Using Complex Vectors," *IEEE Trans. Ind. Appl.*, vol. 35, no. 6, pp. 1424–1432, Nov/Dec 1999.
  - [31] D. N. Zmood and D. G. Holmes, "Stationary Frame Current Regulation of PWM Inverters With Zero Steady-State Error," *IEEE Trans. Power Electron.*, vol. 18, no. 3, pp. 814–822, May 2003.
  - [32] E. Twining and D. G. Holmes, "Grid Current Regulation of a Three-Phase Voltage Source Inverter With an LCL Input Filter," *IEEE Trans. Power Electron.*, vol. 18, no. 3, pp. 888–895, May 2003.
  - [33] K. H. Ahmed, A. M. Massoud, S. J. Finney, and B. W. Williams, "A Modified Stationary Reference Frame-Based Predictive Current Control With Zero Steady-State Error for LCL Coupled Inverter-Based Distributed Generation Systems," *IEEE Trans. Ind. Electron.*, vol. 58, no. 4, pp. 1359–1370, Apr. 2011.
  - [34] H. Lee and V. I. Utkin, "Chattering suppression methods in sliding mode control systems," *Annu. Rev. Control*, vol. 31, no. 2, pp. 179–188, 2007.
  - [35] T. Hornik and Q. C. Zhong, "A current-control strategy for voltage-source inverters in microgrids based on  $H_\infty$  and Repetitive Control," *IEEE Trans. Power Electron.*, vol. 26, no. 3, pp. 943–952, 2011.
  - [36] F.-J. Chang, E.-C. Chang, T.-J. Liang, and J.-F. Chen, "Digital-signal-processor-based DC/AC inverter with integral-compensation terminal sliding-mode control," *IET Power Electron.*, vol. 4, no. 1, p. 159, 2011.
  - [37] A. Abrishamifar, A. A. Ahmad, and M. Mohamadian, "Fixed switching frequency sliding mode control for single-phase unipolar inverters," *IEEE Trans. Power Electron.*, vol. 27, no. 5, pp. 2507–2514, 2012.
  - [38] Y. Yang, K. Zhou, and W. Lu, "Robust repetitive control scheme for three-phase constant voltage constant frequency pulse width modulated inverters," *IET Power Electron.*, vol. 5, no. 6, p. 669, 2012.
  - [39] D. Chen, J. Zhang, Z. Qian, and S. Member, "An Improved Repetitive Control Scheme for Grid-Connected Inverter With Frequency-Adaptive Capability," vol. 60, no. 2, pp. 814–823, 2013.
  - [40] J. Hu, J. Zhu, and D. G. Dorrell, "Model predictive control of grid-connected inverters for PV systems with flexible power regulation and switching frequency reduction," *IEEE Trans. Ind. Appl.*, vol. 51, no. 1, pp. 587–594, 2015.
  - [41] M. P. Kazmierkowski and L. Malesani, "Current control techniques for three-phase voltage-source PWM converters: a survey," *IEEE Trans. Ind. Electron.*, vol. 45, no. 5, pp. 691–703, 1998.
  - [42] A. Bhattacharya and C. Chakraborty, "A Shunt Active Power Filter With Enhanced Performance Using ANN-Based Predictive and Adaptive Controllers," *IEEE Trans. Ind. Electron.*, vol. 58, no. 2, pp. 421–428, 2011.
  - [43] I. Sefa, N. Altin, S. Ozdemir, and O. Kaplan, "Fuzzy PI controlled inverter for grid interactive renewable energy systems," *IET Renew. Power Gener.*, vol. 9, no. 7, pp. 729–738, 2015.
  - [44] D. P. F. Control, C. Tao, S. Member, and C. Wang, "A Design of a DC – AC Inverter Using a Modified ZVS-PWM Auxiliary Commutation Pole and a DSP-Based PID-Like Fuzzy Control," vol. 63, no. 1, pp. 397–405, 2016.
  - [45] J. M. Guerrero, J. Matas, L. Garcia de Vicuna, N. Berbel, and J. Sosa, "Wireless-Control Strategy for Parallel Operation of Distributed Generation Inverters," in *Proceedings of the IEEE International Symposium on Industrial Electronics, 2005. ISIE 2005.*, 2005, vol. 2, pp. 845–850.
  - [46] D. M. Van de Sype, K. De Gussemé, A. P. Van den Bossche, and J. A.

- Melkebeek, "Small-signal Laplace-domain analysis of uniformly-sampled pulse-width modulators," in *2004 IEEE 35th Annual Power Electronics Specialists Conference (IEEE Cat. No.04CH37551)*, 2004, vol. 6, pp. 4292–4298.
- [47] D. Maksimovic and R. Zane, "Small-Signal Discrete-Time Modeling of Digitally Controlled PWM Converters," *IEEE Trans. Power Electron.*, vol. 22, no. 6, pp. 2552–2556, Nov. 2007.
- [48] P. Geng, W. Wu, Y. Ye, and Y. Liu, "Small signal modeling of a novel single-phase photovoltaic inverter," in *2009 IEEE 6th International Power Electronics and Motion Control Conference*, 2009, pp. 2188–2192.
- [49] B.-H. Bae and S.-K. Sul, "A compensation method for time delay of full digital synchronous frame current regulator of PWM AC drives," in *Conference Record of the 2001 IEEE Industry Applications Conference. 36th IAS Annual Meeting (Cat. No.01CH37248)*, vol. 3, pp. 1708–1714.
- [50] D. G. Holmes, T. A. Lipo, B. P. McGrath, and W. Y. Kong, "Optimized Design of Stationary Frame Three Phase AC Current Regulators," *IEEE Trans. Power Electron.*, vol. 24, no. 11, pp. 2417–2426, Nov. 2009.
- [51] D. G. Holmes, B. P. McGrath, and S. G. Parker, "Current Regulation Strategies for Vector-Controlled Induction Motor Drives," *IEEE Trans. Ind. Electron.*, vol. 59, no. 10, pp. 3680–3689, Oct. 2012.
- [52] A. G. Yepes, A. Vidal, J. Malvar, O. Lopez, and J. Doval-Gandoy, "Tuning Method Aimed at Optimized Settling Time and Overshoot for Synchronous Proportional-Integral Current Control in Electric Machines," *IEEE Trans. Power Electron.*, vol. 29, no. 6, pp. 3041–3054, Jun. 2014.
- [53] A. Khairy, M. Ibrahim, N. Abdel-Rahim, and H. Elsharif, "Comparing proportional-resonant and fuzzy-logic controllers for current controlled single-phase grid-connected PWM DC/AC Inverters," in *IET Conference on Renewable Power Generation (RPG 2011)*, 2011, pp. 153–153.
- [54] D. N. Zmood and D. G. Holmes, "Stationary frame current regulation of PWM inverters with zero steady state error," in *30th Annual IEEE Power Electronics Specialists Conference. Record. (Cat. No.99CH36321)*, 1999, vol. 2, pp. 1185–1190.
- [55] R. Teodorescu, F. Blaabjerg, M. Liserre, and P. C. Loh, "Proportional-resonant controllers and filters for grid-connected voltage-source converters," *Electric Power Applications, IEE Proceedings*, vol. 153, pp. 750–762, 2006.
- [56] A. Micallef, M. Apap, C. Spiteri-Staines, J. M. Guerrero, and J. C. Vasquez, "Reactive Power Sharing and Voltage Harmonic Distortion Compensation of Droop Controlled Single Phase Islanded Microgrids," *IEEE Trans. Smart Grid*, vol. 5, no. 3, pp. 1149–1158, May 2014.
- [57] "[CEM - Companhia de Electricidade de Macau] Electricity Supply." [Online]. Available: <http://www.cem-macau.com/Electricity-Supply>. [Accessed: 08-Oct-2015].
- [58] "[CPL Power Hong Kong Limited]. Supply Rules." [Online]. Available: <https://www.clp.com.hk/zh/customer-service/open-and-close-account/supply-rules>. [Accessed: 08-Oct-2015].